**Author(s):** Ibrahim, Hanan H.; Weckman, Timo; Murzin, Dmitry Yu.; Honkala, Karoliina

**Title:** Understanding selective hydrogenation of phenylacetylene on PdAg single atom alloy : DFT insights on molecule size and surface ensemble effects

**Year:** 2024

**Version:** Published version



Ibrahim, H. H., Weckman, T., Murzin, D. Y., & Honkala, K. (2024). Understanding selective hydrogenation of phenylacetylene on PdAg single atom alloy : DFT insights on molecule size and surface ensemble effects. Journal of Catalysis, 434, Article 115523. https://doi.org/10.1016/j.jcat.2024.115523

Journal of Catalysis 434 (2024) 115523

Contents lists available at ScienceDirect

Journal of Catalysis

journal homepage: www.elsevier.com/locate/jcat

Research Article

# Understanding selective hydrogenation of phenylacetylene on PdAg single atom alloy: DFT insights on molecule size and surface ensemble effects

Hanan H. Ibrahim [a], Timo Weckman [a], Dmitry Yu. Murzin [b], Karoliina Honkala [a,*]

[a] Department of Chemistry, Nanoscience Center, University of Jyväskylä, Jyväskylä, 40014, Finland
[b] Faculty of Science and Engineering, Åbo Akademi University, Turku, 20500, Finland

ARTICLE INFO

Dataset link: https://doi.org/10.1016/j.jcat.2024.115523, https://doi.org/10.23729/4fb60b0f-fe7b-4337-b5b0-af3a13f11b6d

*Keywords:*
Density functional theory
Single atom alloy
PdAg
Phenylacetylene

ABSTRACT

Single atom alloys (SAAs) have proven to be effective catalysts, offering customizable properties for diverse chemical processes. Various metal combinations are used in SAAs and Pd dispersed materials are frequently employed in catalyzing hydrogenation reactions. Herein, we explore the hydrogenation of phenylacetylene to styrene and ethylbenzene on PdAg SAA using density functional theory calculations. Our results show that while PdAg SAA does improve the activity of the host Ag towards hydrogenation, a dilute PdAg SAA surface with isolated Pd-atoms is not selective towards partial hydrogenation of phenylacetylene.

Additionally, we investigate how the size of the reactant molecule, the size of the metal alloy ensemble, and the ligand effect impact the hydrogenation process. The SAA enhances the binding strengths of various organic adsorbates, although this effect diminishes as the adsorbate size increases. Our findings indicate the dilute PdAg exhibits selectivity towards hydrogenation of smaller molecules such acetylene due to its distinct adsorption geometry. The selective hydrogenation of phenylacetylene necessitates a surface Pd dimer ensemble. Our research highlights the importance of both reactant molecule size and surface configurations in SAA catalysts. This is particularly crucial when dealing with the adsorption of sizable organic molecules where the functional group can adopt different adsorption modes.

## 1. Introduction

The selective hydrogenation of phenylacetylene (PA) into styrene (ST) holds significant industrial importance, serving as a pivotal process for the production of polymer-grade olefins and the synthesis of various pharmaceuticals and fine chemicals [1–3]. PA is generated as a byproduct during ethylbenzene (EB) dehydrogenation into ST. However, the presence of even trace amounts of PA can potentially poison ST polymerization catalysts due to its high reactivity [4,5]. Traditionally, the conversion of PA to ST has been carried out on noble metal catalysts [4], predominantly using Pd [5–8]. While supported metal catalysts display activity in hydrogenation reactions, they suffer from high cost and poisoning, and, in certain instances, low selectivity. Given the pivotal role of PA hydrogenation in both industrial applications and laboratory settings, there is a on-going demand for better catalysts [5]. Improving the selectivity of PA hydrogenation presents a formidable challenge. This is primarily, because PA is a terminal alkyne, which are typically more reactive than internal alkynes due to the steric accessibility [9].

Single atom alloys (SAAs) have emerged as a new class of heterogeneous catalysts in 2012 [10] and their catalytic potential has been extensively explored over the past decade through a combination of experimental and computational approaches [11–18]. SAAs represent heterogeneous catalytic systems, wherein the thermodynamics of mixing favours the dispersion of an active metal within a less active but more selective host metal. This results in the formation of catalytically active, single atom sites on the host [10,19]. The dispersion of an expensive metal with a cost-effective host metal maximizes the atomic efficiency, provides more uniformly distributed active sites compared to nanoparticle catalysts, and allows for the fine-tuning of the catalytic activity and selectivity [11,14,20]. SAAs have found applications in catalyzing various reactions including hydrogen activation, hydrogenation of unsaturated hydrocarbons and aldehydes, hydrogenolysis of biomass, and dehydrogenation of hydrocarbons and oxygenates [21–25].

Density functional theory (DFT) has been extensively employed to gain microscopic insight on the properties of SAAs and to drive the discovery of new alloys [26–36]. In general, SAAs tend to enhance the binding of various inorganic and organic adsorbates compared to the host metal. These adsorbates encompasses molecules such as $H_2$, $CH_4$, $NH_3$, $CH_3OH$ and $CO_2$. Their binding strengths typically fall between those of monometallic dopant and host metal surfaces [29]. Dopant

* Corresponding author.
*E-mail address:* karoliina.honkala@jyu.fi (K. Honkala).

https://doi.org/10.1016/j.jcat.2024.115523
Received 9 February 2024; Received in revised form 24 April 2024; Accepted 28 April 2024
Available online 30 April 2024

atoms have been shown to reduce the ability of host atoms to bind adsorbates in the vicinity of the SAA site, thus creating a "zone of exclusion" around the dopant atom [32]. This effect becomes more pronounced with more reactive dopant metals, which is attributed to limited mixing of dopant and host metal wave functions, resulting in distinct, single-atom-like electronic states localized on the dopant atom [34].

The hydrogenation of alkyne molecules typically follows the Horiuti–Polanyi mechanism [37], where the hydrogenation begins with the dissociative adsorption of $H_2$, followed by a Langmuir–Hinshelwood type hydrogenation of the reactant in two steps. DFT calculations have shown that SAAs efficiently dissociate $H_2$, resulting in mobile H atoms that subsequently migrate onto the host surface, leaving a single atom site unoccupied [26–28,32,33].

Hydrogenation of acetylene (AC) on SAAs has been extensively studied with a variety of Pd-based SAA catalysts scrutinized for their selectivity towards acetylene partial hydrogenation [23,38–42]. High selectivity (ca. 80%–85%) for partial hydrogenation has been observed on PdCu and PdAg at high conversions, whereas the selectivity on PdAu is notably lower [23,39]. DFT calculations and microkinetic modelling conducted on PdCu [40] align well these experimental results, emphasizing the role of edge and corner sites on reducing the selectivity of PdCu nanoparticles. Furthermore, these studies highlight that maximizing the presence of (111) sites enhances the SAA selectivity towards AC partial hydrogenation [40]. In another study, DFT calculations comparing various Pd-based SAAs ascribe the increased selectivity to charge transfer from the host metals (Ag, Au, Cu) to the Pd dopant. This phenomenon leads to an increase in the electron density at the Pd site, facilitating ethylene desorption due to the repulsion between the nucleophilic ethylene C=C bond and the Pd atom [39]. Furthermore, DFT studies have indicated that isolated metal sites may prevent unwanted reaction pathways. For example, on the Pd(111) surface, the C – C bond breaking and coupling reactions for acetylene compete with acetylene hydrogenation, but they can be suppressed on small Pd ensembles in Ag [43].

Similar to AC, PA partial hydrogenation has been examined both experimentally and computationally [10,12,44]. PdCu and PdZn SAA catalysts have exhibited high selectivity for PA partial hydrogenation [10,12,44,45]. PA hydrogenation on Pd and PdAg alloy catalysts reveals an interesting trend that, while neat Pd demonstrates reasonably high selectivity in PA hydrogenation, alloying Pd with Ag even enhances the selectivity at high conversion [46,47]. However, the Pd-to-Ag ratio in the PdAg alloys tends to be high, which prompts the question of whether active sites are composed of isolated Pd atoms, as occasionally asserted, or if they rather consist of Pd ensembles.

In this study, we explore selective hydrogenation of PA on the $Pd_1Ag(111)$ SAA surface and make comparisons with the hydrogenation on monometallic Pd and Ag surfaces. Additionally, we scrutinize how the size of the reactant molecule and the surface Pd content influence the binding of reactants and the overall hydrogenation process. We achieve this by investigating also the adsorption of acetylene (AC) and diphenylacetylene (DPA) and their derivatives as well as by examining the initial hydrogenation steps of AC and ethylene (ET) on $Pd_1Ag(111)$ SAA surfaces with varying Pd content.

Our findings indicate that a sparsely populated SAA surface with isolated Pd-atoms should not exhibit selectivity towards the partial hydrogenation of PA. However, when the surface features Pd dimer ensembles, the hydrogenation process can become selective. Furthermore, our results demonstrate that the size of the alkyne impacts the binding to the SAA. Although the SAA generally enhances the binding of the reactant molecules, this effect diminishes as the size of a reactant molecule increases. The molecule size effect has significant implications for the hydrogenation process, as the stronger bonding of AC leads to selective hydrogenation of AC even in the case of dilute PdAg SAA (see Fig. 1).

## 2. Computational details

The electronic structure calculations were conducted using the density functional theory as implemented in the GPAW [48,49]. The Kohn–Sham equations were solved using a plane wave basis set with an energy cutoff of 500 eV. The exchange–correlation functional was approximated using the Perdew–Burke–Ernzerhof (PBE) functional [50] with the D3 dispersion correction proposed by Grimme [51–53]. A $9 \times 9 \times 9$ k-point sampling was used for the bulk metal systems, while a $6 \times 7 \times 1$ mesh was used for the small $2 \times 2$ surface cell and a sparser $3 \times 3 \times 1$ mesh was for the larger $3 \times 3$ and $4 \times 4$ surface cells. Adsorption energies, $E_{ad}$, are calculated using the following equation:

$$E_{ad} = E_{tot} - E_{surf} - E_{ads}^{gas} \quad (1)$$

where $E_{tot}$ is the total energy of the surface and the adsorbed molecule, $E_{surf}$ is the energy of the bare surface and $E_{ads}^{gas}$ is the energy of the adsorbed molecule. The transition states were determined using the climbing image nudged elastic band method (CI-NEB) [54,55] with the FIRE [56] optimizer. All with forces converged to below 0.05 eV $Å^{-1}$. Vibrational analysis was carried out for the highest energy images to ensure the obtained configuration corresponded to a true transition state.

The lattice constants of Pd and Ag were calculated to be 3.89 Å and 4.07 Å, respectively, which agree well with the experimental lattice constants (3.89 Å for Pd and 4.09 Å for Ag) [57]. A periodic slab was used to model the surface environment. The FCC(111) surfaces were modelled with the $3 \times 3 \times 5$ slabs having the bottom two layers constrained to conserve the bulk geometry. A vacuum layer of 10 Å was used above and below the slab. The $Pd_1Ag$ SAA surface was created from the Ag(111) surface by replacing one of the surface Ag atoms with a Pd atom.

For calculations involving larger molecules, a $4 \times 4$ simulation cell was used. To reduce the computational burden, the slab thickness was decreased from five to three layers. Reducing the slab thickness had a relatively large effect on the Pd(111) surface, where the adsorbates bonded the strongest, by deviating by as much as 0.42 eV from the five layer slab. However, on the Ag(111) and $Pd_1Ag(111)$ surfaces where the adsorbate–surface interaction was weaker, the adsorption energies deviated only up to 0.06 eV from the adsorption energies obtained on the $3 \times 3 \times 5$ slab.

### 2.1. Free energy calculations

The free energies of the hydrogenation pathways were computed to study the hydrogenation pathway at finite temperature and were also used for the selectivity descriptors discussed below in detail.

We define the Gibbs free energy for the gas-phase species as

$$G_{TK} = E_{tot} + E_{ZPE} + \sum_{\nu} \frac{h\nu}{e^{\frac{h\nu}{KT}} - 1} + \int_0^T C_p dT - T(S_{vib} + S_{rot} + S_{trans}), \quad (2)$$

where $E_{tot}$ is the total electronic energy, $E_{ZPE}$ is the zero point energy, $\sum_{\nu} \frac{h\nu}{e^{\frac{h\nu}{KT}} - 1}$ is the vibrational contribution to the internal energy at the temperature $T$, $C_p$ is the heat capacity of the gas and $S_{vib}, S_{rot}$ and $S_{trans}$ are the entropy contributions corresponding to vibrational, rotational and translational degrees of freedom. The thermodynamic quantities were computed using the thermochemistry toolkit available in ASE [58].

For the adsorbed species, the Gibbs free energy was defined in the harmonic limit, where only the vibrational contributions of the molecules were included in the entropy,

$$G_{TK} = E_{tot} + E_{ZPE} + \sum_{\nu} \frac{h\nu}{e^{\frac{h\nu}{KT}} - 1} - TS_{vib}. \quad (3)$$

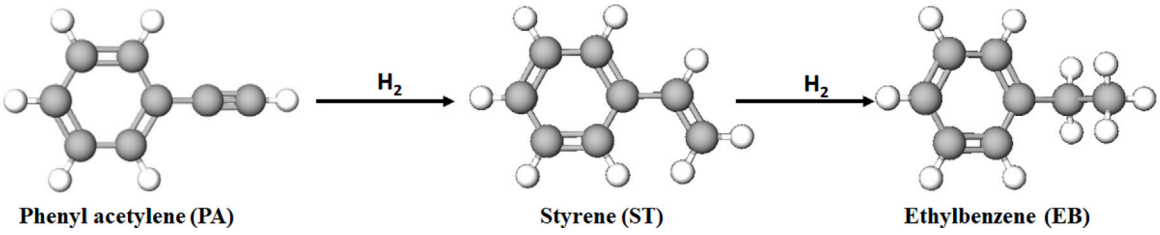


**Fig. 1.** The hydrogenation pathway for phenylacetylene.

However, care should be taken when comparing computed free energies to measured ones, as some of the hydrogenation are carried out in liquid phase [5,44,59]. Adsorption from a liquid phase would presumably lead to a smaller loss of entropy due to the lower entropy of the liquid phase in general.

Hydrogenation selectivity is quantified using the selectivity descriptors as proposed by Xu et al. [60] The descriptor is defined as free energy difference between desorption free energy $G_{des}$ and activation free energy barrier $G_{TS}$ as follows

$$\Delta G_{\mathrm{des}} = 0.5 \times G_{\mathrm{H_2}} + G^{\mathrm{gas}}_{\mathrm{mol}} + G_{\mathrm{surf}} - G_{\mathrm{mol*+H*}}$$
$$\Delta G_{\mathrm{TS}} = (G_{\mathrm{mol*+H*}})_{\mathrm{TS}} - G_{\mathrm{mol*+H*}}$$
$$\Delta\Delta G = \Delta G_{\mathrm{TS}} - \Delta G_{\mathrm{des}}$$

with asterisk denoting an adsorbed species and mol corresponds to the reactant molecule. Positive $\Delta\Delta G$ values stand for desorption being more likely than forward hydrogenation, while for negative $\Delta\Delta G$ values, the opposite is true. For the hydrogenation process to exhibit selectivity, the hydrogenation step of the alkyne must be active ($\Delta\Delta G < 0$), while the subsequent hydrogenation step of the alkene should not take place ($\Delta\Delta G > 0$).

### 2.2. Deformation energies

To analyse the strength of the adsorbate–surface bond, we consider the electronic interaction energy determined as [61]

$$E_{\mathrm{int}} = E_{\mathrm{tot}}(\mathrm{mol + surf}) - E_{\mathrm{tot}}(\mathrm{mol}) - E_{\mathrm{tot}}(\mathrm{surf}). \quad (4)$$

$E_{\mathrm{tot}}(\mathrm{mol + surf})$ is the total energy for the optimized adsorbate–surface system and $E_{\mathrm{tot}}(\mathrm{mol})$ and $E_{\mathrm{tot}}(\mathrm{surf})$ are the total energies for frozen geometries for the molecule and the surface respectively obtained by optimizing the adsorbate–surface system.

The deformation energy measures structural distortion on the adsorbate and/or the surface due to adsorption. It can be computed separately for both species and is defined as the energy difference between a relaxed adsorbate (or surface) geometry upon adsorption and a relaxed gas-phase adsorbate (or bare surface) in fully relaxed geometry,

$$E_{\mathrm{def}} = E^{\mathrm{mol}}_{\mathrm{def}} + E^{\mathrm{surf}}_{\mathrm{def}} \quad (5)$$
$$E^{\mathrm{mol/surf}}_{\mathrm{def}} = E_{\mathrm{tot}}(\mathrm{mol/surf}) - E_{\mathrm{tot}}(\mathrm{mol/surf})^{\mathrm{relaxed}}. \quad (6)$$

The adsorption energy is the sum of both the electronic interaction and the deformation energies.

## 3. Results and discussion

### 3.1. Dissociative adsorption of $H_2$

The dissociative adsorption of molecular hydrogen on the Ag(111) surface is thermoneutral but highly activated featuring a barrier of 0.92 eV (Table 1). This barrier is slightly lower than the previously reported value of 1.15 eV [22]. Due to the high $H_2$ dissociation barrier, the Ag(111) surface is inactive for hydrogenation reactions. In contrast, the Pd(111) surface exhibits the opposite behaviour, readily dissociating $H_2$ with an reaction energy of −1.24 eV. This aligns with the previously calculated value of −1.23 eV [22]. Compared to Ag(111), the $Pd_1Ag$ SAA significantly enhances $H_2$ adsorption. In addition to mildly exothermic molecular adsorption, the dissociation reaction energy is also exothermic, and the activation energy is substantially reduced to only 0.21 eV. In this process, the hydrogen atoms occupy the hcp and fcc hollow sites next to the Pd atom, surrounded by Ag atoms. These findings are consistent with earlier DFT results for $H_2$ dissociation on $Pd_1Ag$ SAA [22], highlighting significant enhancement of $H_2$ dissociation in the presence of a Pd dopant atom. However, we note that DFT calculations tend to overestimate the binding of $H_2$ on metal surfaces [62,63]. The experimental heat of adsorption for $H_2$ on Pd(111) [64] is only −0.90 eV being 0.28 eV less exothermic than our computed value when including the ZPE correction. For a detailed benchmark of PBE+D3 on larger compounds on metal surfaces, see section S1 in the Supplementary Information.

Additionally, we explored the potential of a Pd monomer to induce hydrogen spillover to Ag sites, which may impact overall catalytic efficiency [65]. The spillover from a Pd-Ag hollow site to the nearest Ag hollow site has a thermodynamic barrier of 0.3 eV, which is accessible in the process conditions. Given the low spillover barrier, we assume the hydrogens spill over onto the host metal and the hydrogenation proceeds one hydrogen at a time.

### 3.2. Adsorption of the organic molecules

Multiple adsorption geometries and molecular conformations were screened for phenylacetylene (PA), styrene (ST), and ethylbenzene (EB) molecules on the studied surfaces by exploring different adsorption sites for the triple or double bonds and screening the most favourable orientation for the molecule. Fig. 2 depicts the most stable adsorption structures, and Table 2 provides a summary of corresponding adsorption energies. In general, adsorption is weakest on the Ag(111) surface and strongest on the Pd(111) surface. However, on PdAg(111), the presence of a Pd monomer enhances adsorption compared to the host metal, although it remains weaker than on Pd(111).

Our results on Ag(111) show that PA, ST, and EB do not exhibit a strong preference for any particular adsorption site, as their adsorption energy vary only slightly from one site to another. The adsorption energies for all three molecules are approximately −1 eV predominantly attributed to weak van der Waals (vdW)-interactions. Adsorption energies computed without vdW interactions are close to zero (see Table 2). The weak interaction is also evident in the long adsorbate–surface distances depicted in Fig. 2, as well as the fact that the adsorbate maintains its gas-phase geometry.

On Pd(111), the adsorption energies are over 1 eV more exothermic ranging from −2.8 eV (PA) to −2.0 eV (EB). The adsorbate–surface interaction on Pd exhibits a significant covalent contribution, arising from the interaction between the $\pi$ and $\pi^*$ orbitals of the benzene ring and the surface $d$-orbitals through the donation and backdonation mechanism [66]. Fig. 2 visually illustrates how this covalent interaction substantially distorts the planar benzene ring and elongates the linear C≡C bond from its gas-phase value of 1.21 Å to 1.37 Å. Considering the highly exothermic nature of adsorption onto the Pd(111) surface,

**Table 1**
$H_2$ adsorption, activation, and dissociation energies on Pd(111), Ag(111), and $Pd_1Ag$ (111) surfaces. The values in the parenthesis have been obtained from Ref. [22] for reference.

| Surface | $H_2$ adsorption energy $E_{ad}$ (eV) | Activation barrier $E_a$(eV) | Binding Energy $E_b$(eV) |
|---|---|---|---|
| Ag(111) | −0.07 | 0.92 (1.15) | 0.00 (0.31) |
| Pd(111) | – | 0.00 (–) | −1.24 (−1.23) |
| $Pd_1Ag$ SAA | −0.34 | 0.21 (0.31) | −0.48 (−0.33) |

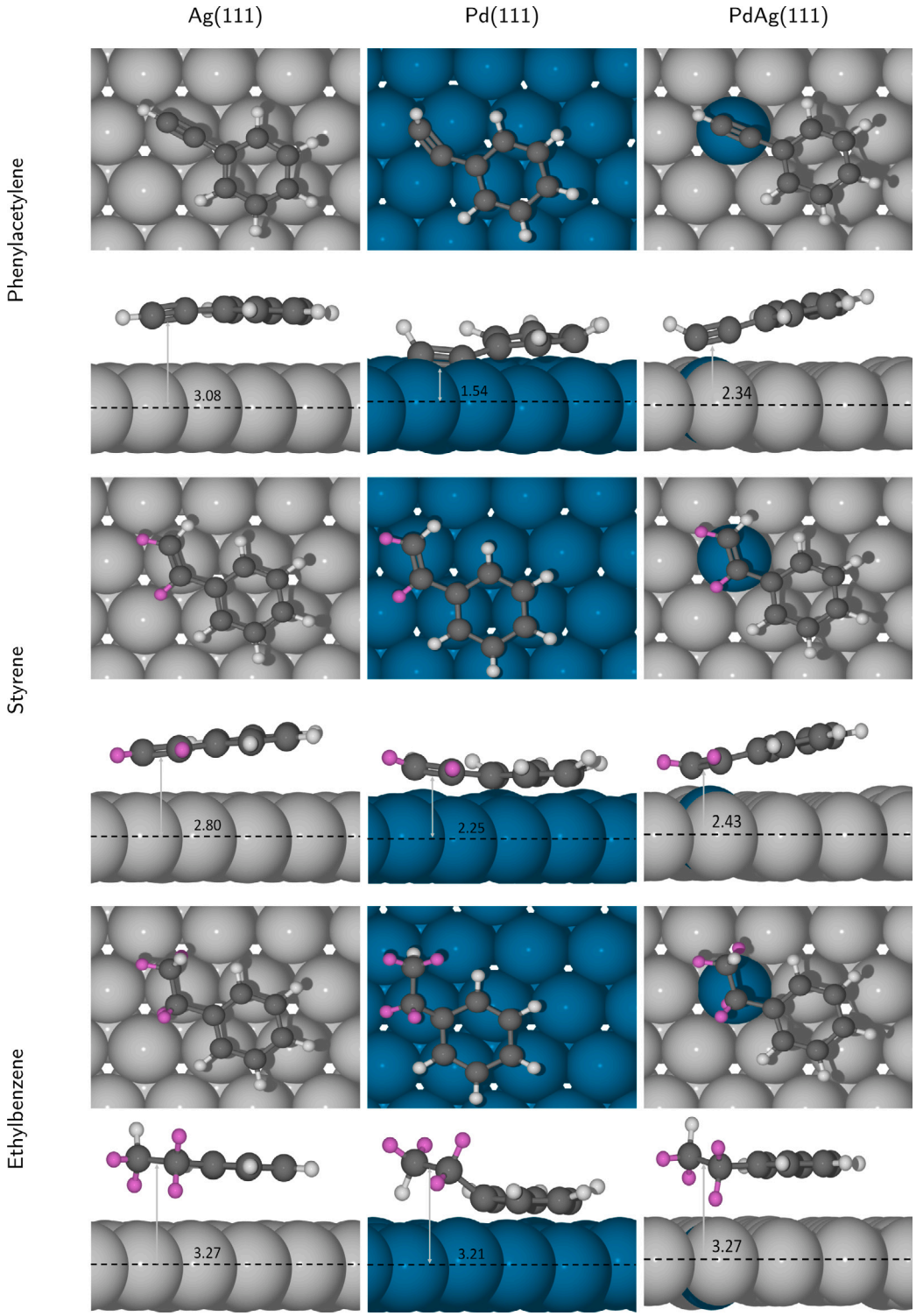


**Fig. 2.** The optimal adsorption geometries for PA (upper row), ST (middle) and EB (lower) adsorbed onto Ag(111) (left column), Pd(111) (center) and PdAg(111)SAA (right) surfaces. On Ag(111) and $Pd_1Ag$ SAA surfaces, the ontop site is the most stable adsorption site for C−C bond, however, the 3-fold hollow site is more favourable for C−C bond of PA and EB on the Pd(111) surface. The side view shows the vertical distance between the top layer of the metal surface and the midpoint of the C−C bond in angstroms. The hydrogen atoms added during hydrogenation are highlighted in pale violet.

**Table 2**
The computed adsorption energies, $E_{ad}$, of phenylacetylene, styrene and ethylbenzene on Pd(111), Ag(111), and $Pd_1Ag(111)$. The numbers in parenthesis are single point values computed with the PBE functional and excluding the van der Waals -correction. All values are given in eV.

| Surface | Adsorption energy $E_{ad}$ (eV) | | |
|---|---|---|---|
| | Phenylacetylene | Styrene | Ethylbenzene |
| Pd(111) | −2.76 (−1.63) | −2.48 (−1.22) | −2.03 (−0.96) |
| Ag(111) | −0.95 (−0.06) | −1.07 (−0.06) | −1.03 (−0.05) |
| $Pd_1Ag(111)$ SAA | −1.28 (−0.33) | −1.37 (−0.27) | −1.15 (0.08) |

**Table 3**
The computed activation barriers for each PA hydrogenation step into EB through ST on Pd(111), Ag(111), and $Pd_1Ag(111)$ surfaces. The reaction energy $\Delta E_r$ of each step is given in the parenthesis. All values are in eV.

| Surface | Activation energy $E_a$ (eV) ($\Delta E_r$) | | | |
|---|---|---|---|---|
| | TS1 | TS2 | TS3 | TS4 |
| Pd(111) | 0.68 (−0.15) | 0.82 (−0.84) | 0.87 (−0.09) | 0.75 (0.06) |
| Ag(111) | 0.54 (−0.95) | 0.35 (−1.57) | 0.63 (−0.32) | 0.35 (−1.28) |
| $Pd_1Ag(111)$ SAA | 0.44 (−1.10) | 0.25 (−1.00) | 0.38 (−0.40) | 0.25 (−0.85) |

we investigated the influence of surface coverage by implementing a smaller 2 × 2 surface model to simulate higher surface coverage. As the simulation cell size decreased, allowing interaction between the molecule and its periodic images, both PA and ST adopted a vertical orientation, binding to the surface solely through the carbon tail (see Figure S1 in Supplementary Information). At high coverage, the adsorption energy for PA is computed to be −2.62 eV, slightly less exothermic compared to the low coverage value. However, ST adsorption weakens considerably with a adsorption energy being only −1.42 eV.

Similarly to hydrogen adsorption, $Pd_1Ag(111)$SAA enhances the adsorption of the organic species compared to the Ag(111) surface, resulting in adsorption energies that are approximately 0.15 eV - 0.30 eV more exothermic. Without the vdW correction, adsorption energies are only mildly exothermic. Since the phenyl ring does not interact with the Ag surface, the adsorption bond is formed via the C≡C and C=C bonds of PA and ST, respectively.

Recent DFT calculations for PA adsorption on $Pd_1Cu(111)$ SAA predict that PA adsorbs at the Pd-Cu interface with the C≡C bound to the Pd-Cu bridge site with an adsorption energy of −0.99 eV, whereas ST binds ontop the Pd-atom with an adsorption energy of −0.28 eV [12]. The DFT calculations conducted on PdCu were performed without considering a dispersion interaction correction. These results should be compared to the values presented in Table 2 where the dispersion interaction has been omitted. We see that the binding of PA on PdAg is significantly weaker than that on PdCu, whereas ST binding is similar in magnitude.

### 3.3. Phenylacetylene hydrogenation

The full hydrogenation pathway from PA to EB was thoroughly investigated on all three surfaces. It is assumed that the hydrogenation process begins with the terminal carbon, followed by the hydrogenation of the $\alpha$-carbon, in agreement with previous computational studies [67]. Table 3 presents the computed activation and reaction energies for the hydrogenation steps, while the co-adsorption energies for hydrogen and the organic reactants can be found in Table S2 in the Supplementary Information. Fig. 4 illustrates the initial, transition and final states for each elementary step on the $Pd_1Ag$ SAA. Corresponding structures for Ag and Pd surfaces are available in the Supplementary Information.

Additionally, a free energy surface for the complete PA hydrogenation at 300 K is provided in Fig. 3. Remarkably, the hydrogenation free energy barriers remain below 0.8 eV on all surfaces. When comparing the free energy pathway on the three surfaces, it is notable that the addition of an hydrogen atom varies across the three steps: on Pd(111) the free energy decreases when a hydrogen is introduced into the system, while on Ag(111) and PdAg SAA the free energy increases. This difference arises for two reasons: Firstly, hydrogen binding is highly exothermic on Pd(111), weakly exothermic on PdAg SAA, and energy neutral on Ag(111). Secondly, on Pd(111), the hydrogen atom can co-adsorb further away from the organic species, whereas on PdAg SAA both reactants co-adsorb onto the active site, leading to some adsorbate–adsorbate repulsion.

On Ag(111), due to the weak adsorbate–surface interaction for both PA and ST, the adsorbates retain their gas-phase geometry and remain at approximately 3 Å above the surface. We find that the activation (free) energies for hydrogenation on Ag(111) are relatively low and attainable at the process conditions. For ST, the barrier of the first hydrogenation step (TS3) is 0.63 eV, which is slightly higher (0.1 eV) compared to the barrier for PA (TS1). However, both molecules exhibit similar barriers of 0.35 eV for the second hydrogenation step. In the case of PA, after the first hydrogenation of PA, the $\alpha$-carbon undergoes a transition from $sp$-hybridization to $sp^2$ hybridization. This transition allows the $\alpha$-carbon to deviate from the linear structure of the triple bond and to bend down to form a covalent bond with surface. Consequently, this step results in a highly exothermic reaction energy for the first hydrogenation step. A similar mechanism is observed on the $Pd_1Ag(111)$ SAA surface (see Fig. 4).

On Pd(111), the activation barriers for hydrogenation are generally higher than on Ag(111), likely due to the stronger adsorbate–surface interaction. Although the second hydrogenation step typically has lower activation energy than the first step, this is not true for PA on Pd(111). Specifically, the activation energy for step TS2 is 0.82 eV, exceeding that of step TS1 with a barrier of 0.68 eV. Additionally, the reaction energies for the hydrogenation on Pd(111) are not as exothermic as those on Ag(111) and $Pd_1Ag(111)$ SAA surfaces (see Table 3). This difference stems from the degree of hybridization between the metal surface and the triple/double bond of the carbon tail. On the Pd(111) surface, the carbon atoms in PA are already hybridized with the Pd surface, while on the other surfaces, this hybridization occurs subsequent to the initial activation of carbons through the first hydrogenation step.

The activation energies on $Pd_1Ag(111)$ SAA demonstrate that the Pd atom improves on the activity of the Ag host, resulting in a decrease in activation energies of at least 0.1 eV for all hydrogenation steps. Unlike on the monometallic surfaces, the activation energy of the first hydrogenation step for ST (TS3) is lower than that for PA (TS1), making the hydrogenation of ST more facile than PA. All hydrogenation reactions take place at the active Pd site, with the reacting C−C bond positioned above the Pd-atom, as the organic molecules are repelled by the Ag host. This is in contrast to PA hydrogenation on PdCu SAA, where the PA hydrogenation has been reported [12] to occur at a bridge site adjacent to the Pd-dopant. However, it is worth noting that the computed activation energies for the PdCu SAA are approximately twice as high as those reported here for the PdAg SAA.

### 3.4. Selectivity of phenylacetylene hydrogenation

The desired product of PA hydrogenation is ST, not the fully hydrogenated EB. Therefore, achieving selective hydrogenation is important. We quantify the rates of various competing reactions using selectivity descriptors such as those proposed in Xu et al. [60] or by comparing the relative free energy barriers for forward hydrogenation and desorption steps [40]. Typically, the selectivity analysis focuses on a specific molecule, in our case, that is the alkene intermediate ST, while other molecules are often disregarded. This approach implicitly assumes that under the given reaction conditions, the formation of a studied intermediate takes place (in our case the hydrogenation of PA to ST). However, this assumption may not always hold, and it is essential to determine the relative selectivity of both PA and ST hydrogenation steps.

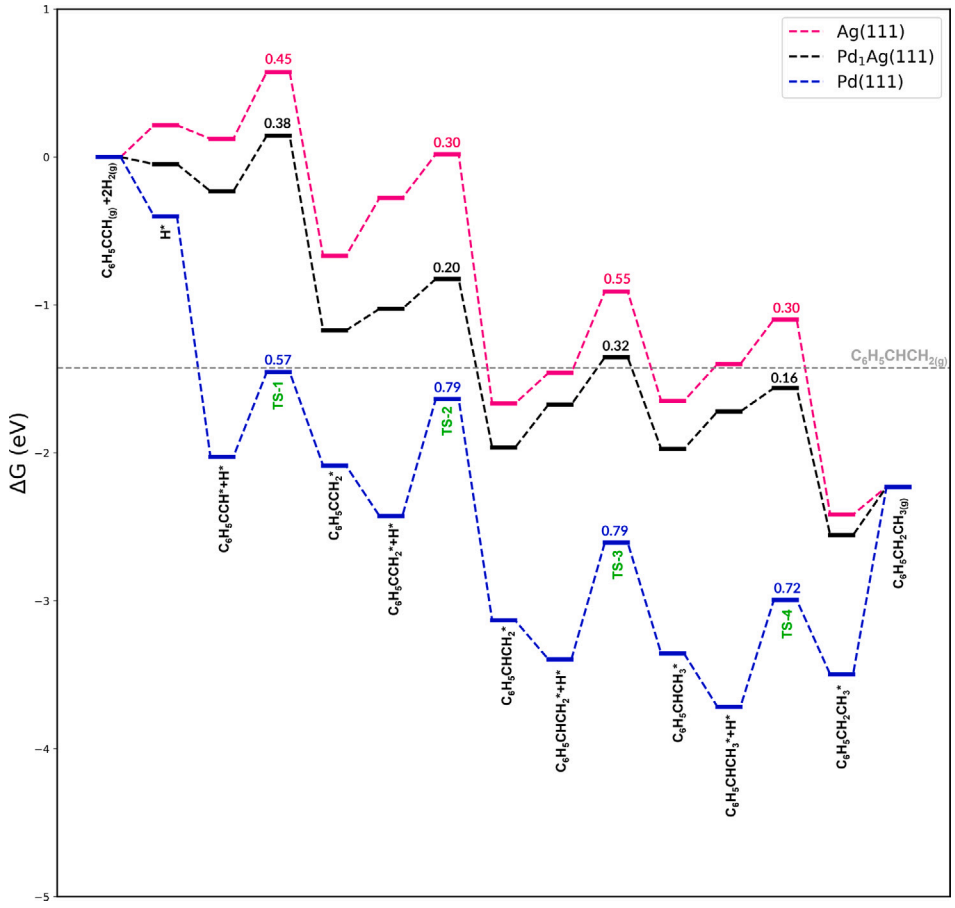


**Fig. 3.** The free energy diagram for PA and ST hydrogenation over Ag(111) (red), $Pd_1Ag$ SAA (black) and Pd(111) (blue) surfaces. The free energies are computed at 300 K temperature and all the gas-phase species have the partial pressure of 0.1 bar. The asterisk represents an active surface site. At each hydrogenation step, one hydrogen adsorbs onto the surface.

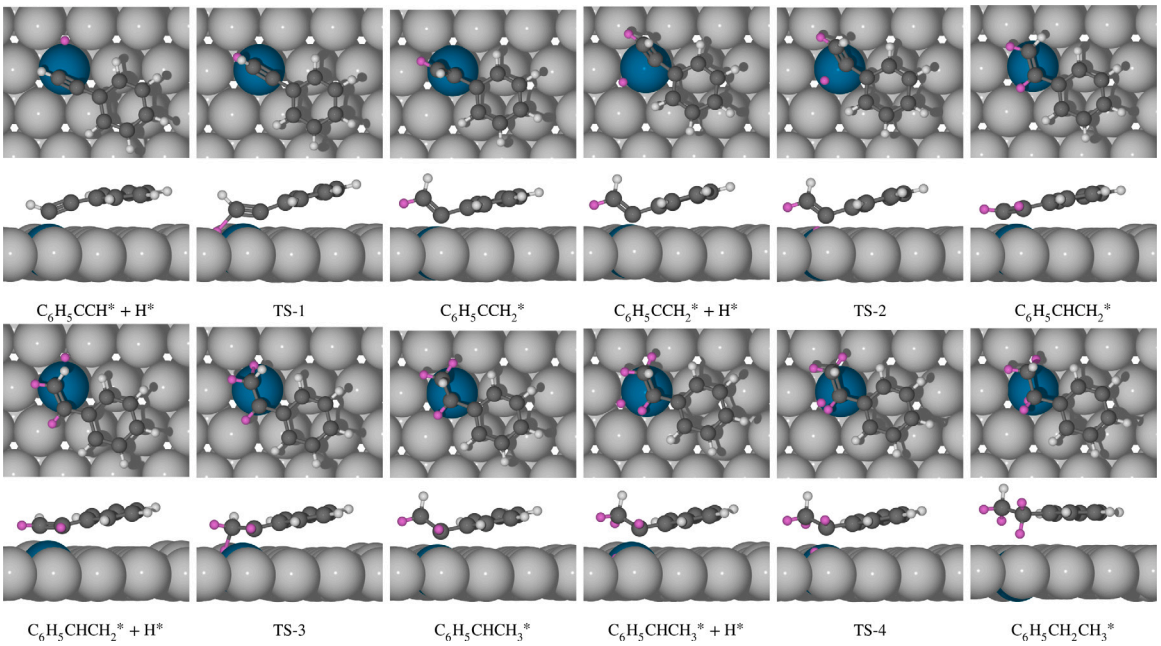


**Fig. 4.** The calculated hydrogenation pathways for PA ($C_6H_5CCH$) and ST ($C_6H_5CCH_2$) on $Pd_1Ag(111)$SAA. Each step represents one hydrogenation step as depicted on the free energy surface in Fig. 3.

**Table 4**
Selectivity descriptors for PA and ST at 300 K and 0.1 bar partial pressure for the reaction components. An asterisk indicates that selective PA conversion to ST could be achieved at a higher temperature. The values given in parentheses are the free energy of desorption and selectivity at high coverage. All values in eV.

| Descriptor | Pd(111) | Ag(111) | $Pd_1Ag(111)$ SAA |
|---|---|---|---|
| Phenylacetylene | | | |
| $\Delta G_{TS}$ | 0.57 | 0.44 | 0.38 |
| $\Delta G_{des}$ | 2.03(1.80) | −0.12 | 0.23 |
| $\Delta\Delta G^{PA}$ | −1.46(−1.23) | 0.56 | 0.15 |
| Styrene | | | |
| $\Delta G_{TS}$ | 0.79 | 0.55 | 0.32 |
| $\Delta G_{des}$ | 1.96(0.59) | 0.02 | 0.24 |
| $\Delta\Delta G^{ST}$ | −1.17 (0.20) | 0.53 | 0.08 |
| Selective for ST | No* (Yes) | No | No |

Upon analysing Fig. 3, we note that for ST, the barrier for forward hydrogenation is higher than the desorption barrier (indicated by the horizontal grey dashed line) on Ag(111) but not on $Pd_1Ag(111)$. This discrepancy suggests a selectivity of PA hydrogenation towards ST on Ag, whereas on PdAg SAA, the selectivity is less distinct. It is important to emphasize that the PA desorption barrier is lower than the forward hydrogenation barrier on both Ag(111) and $Pd_1Ag(111)$. Thus, our calculations indicate the absence of PA hydrogenation under the given reaction conditions.

Estimating the selectivity from free energy landscape alone can be challenging when dealing with multiple molecules and surfaces. To systematically evaluate the selectivity of the hydrogenation process, we utilize the selectivity descriptor model as described in the Computational details section. The selectivity descriptors presented here are calculated at 300 K and 0.1 bar, and they are summarized in Table 4. By comparing the descriptor for both PA and ST, we can assess whether the hydrogenation process exhibits selectivity on the given substrate.

On Pd(111), the $\Delta\Delta G$ values are negative for both molecules, suggesting that PA fully hydrogenates into EB at the specified temperature and at low surface coverage. Since the $\Delta\Delta G$ value for PA is lower compared to the corresponding value for ST, achieving the desired selectivity might be possible at higher temperatures or at high surface coverage, where PA adsorption is significantly favoured over ST. Assuming that the PA/ST hydrogenation barriers remain relatively unaffected by the surface coverage, we included the free energy barrier for desorption at high surface coverage on Pd(111) in Table 4. Due to substantial disparity in binding energies between PA and ST, the Pd(111) exhibit selectivity to partial hydrogenation at high surface coverage. A similar effect of surface coverage on the adsorption and reaction selectivity on Pd(111) has been previously reported for acrolein [68]. Table 4 showcases comparable $\Delta\Delta G$ descriptor values for both PA and ST on Ag(111) and $Pd_1Ag$ SAA surfaces. This similarity indicates an equivalent reactivity of both molecules on these metal surfaces. Consequently, varying the reaction temperature may not lead to an improvement in selectivity.

Within our calculations, the Pd(111) surface serves as a reference for our SAA system and under hydrogenation conditions it typically has subsurface hydrogen $PdH_x$. However, examining the influence of $PdH_x$ on PA hydrogenation lies beyond the scope of this study. Prior DFT studies on acetylene hydrogenation have shown [69,70] that the formation of subsurface hydrogen tends to lower the activation energies of the hydrogenation steps while simultaneously weakening the adsorption of reactants. Analogous effects may influence PA hydrogenation activity on Pd(111).

Recent studies on PA hydrogenation over PdCu SAA catalysts have demonstrated very high selectivity towards ST [12,44]. DFT calculations indicate that the Cu-host actively binds both PA and ST molecules [12], in contrast to the Ag-host, which we find rather inert. Comparison of PA and ST adsorption energies on PdCu and PdAg reveals a clear distinction between these SAAs. PdCu binds PA more strongly but ST more weakly, while the opposite holds for $Pd_1Ag$ and Ag.

Previous experimental results on PA hydrogenation on PdAg alloys show that the catalysts exhibit excellent selectivity towards the production of styrene. At low conversion, the selectivity on Pd and PdAg are similar, but the selectivity on Pd tends to drop at high conversion, while PdAg remains highly selective even at high conversion of PA [8,9,46,47,71].

The Pd:Ag ratio in the experimental systems is relatively high and it is reasonable to ask, whether ensembles of Pd-atoms on the surface, such as dimers or trimers, play a role in the hydrogenation process. While the surface of PdAg alloys tends to be terminated by Ag atoms, spectroscopy measurements on adsorbed CO on PdAg surfaces have shown that the formation of isolated Pd-sites on a surface take place only on low Pd surface coverage, typically below 0.002 monolayer [72]. The CO adsorption peak at 2050 $cm^{-1}$ is attributed to CO adsorption ontop a Pd atom, representing a dominating mode. A smaller peak at 1950 $cm^{-1}$ is commonly detected, associated with CO adsorption on a Pd–Pd bridge site [72–74]. Surface Pd atoms easily cluster into dimers and larger Pd ensembles, a phenomenon that can be driven by adsorbate-induced segregation [72–74]. Since the Pd dimer adsorption peak is present even at Pd:Ag ratio of 1:2 [75], we investigate whether the Pd dimer could be responsible for the observed selectivity.

It has been demonstrated that PdAg single atom alloy catalysts with isolated Pd sites exhibit high selectivity for the partial hydrogenation of acetylene [23]. In this experimental study, Ag:Pd ratios range form 40 to 200 and the obtained results reveal that the pre-reduction temperature of catalysts significantly influences the Pd distribution on the surface, with reduction at high temperatures resulting in isolated, single atom Pd sites. These catalysts show excellent selectivity towards the partial hydrogenation of AC. Moreover, the activation energy for AC hydrogenation was measured to be lower on the dilute PdAg catalyst than on the neat Pd catalyst. Given that dilute PdAg SAA exhibits activity and selectivity towards the partial hydrogenation of AC, we investigate whether the size of the reactant molecule affects the adsorption thermodynamics or the hydrogenation kinetics on a SAA catalyst.

To address these aspects, we first examine AC and DPA adsorption on the dilute PdAg SAA surface to investigate the molecule size effect on adsorption. Additionally, we compare hydrogenation kinetics between AC and PA. Following this, we analyse how variations in Pd concentration impact the adsorption thermodynamics and hydrogenation kinetics of AC, PA and DPA.

### 3.5. Molecule size effect

Firstly, we explored the optimal adsorption geometries of acetylene and diphenylacetylene by screening various conformations and adsorption sites. Subsequently, the activation energies for the selectivity determining AC and ET hydrogenation steps were computed. A detailed discussion on these calculations can be found in Section S6 in the Supplementary Information.

Table 5 presents the adsorption energies of above mentioned molecules together with PA and its derivatives on Ag(111) and $Pd_1Ag$ SAA. It is evident that adsorption energies become more exothermic as the size of molecule increases, primarily due to attractive van der Waals -interaction between the phenyl ring and the surface. To assess the influence of the SAA on binding characteristics of these molecules, we compare adsorption energies and geometries on Ag(111) and $Pd_1Ag$ surfaces. The results clearly indicate that SAA enhances adsorption for all the molecules. However, the impact of the SAA is smaller for the larger molecules. Specifically, for AC, PA and DPA, the adsorption energies are more exothermic by 0.60, 0.33 and 0.18 eV on the $Pd_1Ag$ SAA compared to Ag(111), respectively. This trend also applied to the double bonded species (see Fig. 6).

**Table 5**
The adsorption and deformation energies $E_{ads}$ for the organic molecules on $Pd_1Ag$ SAA surface. $\Delta\Delta E_{ads}$ is the difference between the adsorption energies on Ag(111) and $Pd_1AgSAA$ and $E_{def}^{mol}$ is the deformation energy of the adsorbate molecule on the $Pd_1AgSAA$ surface. For comparison, the adsorption energies for PA, ST and EB from Table 2 are also tabulated here. All values are given in eV.

| Molecule | $Pd_1Ag$ SAA | Ag(111) | $\Delta\Delta E_{ads}$ | $E_{def}^{mol}$ |
|---|---|---|---|---|
| AC (bridge) | −0.90 | −0.30 | 0.60 | 2.04 |
| AC (ontop) | −0.82 | – | – | 0.71 |
| ET | −0.84 | −0.42 | 0.42 | 0.41 |
| Ethane(EA) | −0.45 | −0.32 | 0.13 | 0.02 |
| PA | −1.28 | −0.95 | 0.33 | 0.50 |
| ST | −1.37 | −1.07 | 0.30 | 0.45 |
| EB | −1.15 | −1.03 | 0.12 | 0.03 |
| DPA | −1.55 | −1.37 | 0.18 | 0.41 |
| CST | −1.65 | −1.58 | 0.07 | 0.26 |
| TST | −1.70 | −1.65 | 0.05 | 0.44 |
| BB | −1.71 | −1.66 | 0.05 | 0.01 |

The heat of adsorption has been measured for ET on a dilute $Pd_{0.025}Ag$ SAA using microcalorimetry [23], ranging at low ET surface coverage from −0.99 eV on an Ag surface with Pd ensembles to −0.64 eV on an Ag surface with isolated Pd atoms. The extent to which the Pd-atoms were allowed to form ensembles was controlled by the pre-reduction temperature of the catalysts. Our calculations give an adsorption energy of −0.84 eV for ET on $Pd_1Ag$ SAA which is somewhat more exothermic than the experimentally measured value on isolated Pd sites, while the ET adsorption on the Pd dimer was calculated to be −0.92 eV. The zero-point energy contribution has only a small effect on the adsorption energy, increasing the adsorption energy to −0.80 eV on $Pd_1Ag$ SAA and to −0.90 eV on Pd dimer.

The molecule size also influences the favoured adsorption geometry. While PA and DPA prefer the on-top-Pd-atom site, AC binds at the Pd-Ag interface in the bridge position, which is 0.08 eV more stable than the on-top position. This stabilization is crucial for hydrogenation selectivity as it makes AC slightly more stable than ET. While the energy difference between these two geometries is relatively small, the electronic interaction between the AC and the $Pd_1Ag$ SAA surface is significantly stronger on the bridge site (please, see Figure S6 in the Supplementary Information). This results in a significant distortion of the linear structure of the AC (Figure S6) and a substantial deformation energy (~2 eV). In contrast, the deformation energy at the on-top site is modest, less than 0.5 eV. Please refer to Table 5 for a summary of deformation energies for all the investigated molecules.

To address the impact of molecule size on selectivity, we computed activation energies for the initial hydrogenation steps of both AC and ET on $Pd_1Ag$ SAA. They are shown in Table S12 and comparable to those calculated for PA and ST. This indicates that the size of a molecule does not affect the hydrogenation barrier. Furthermore, the selectivity descriptors for AC and ET determined at 230 K and 1 bar (see Table 6) demonstrate selectivity for partial hydrogenation. Specifically, $\Delta\Delta G^{AC}$ is lower than $\Delta\Delta G^{ET}$ the for ET, indicating preference for AC over ET. This selectivity can be attributed to the stronger adsorption of AC relative to ET as well as the careful selection of reaction conditions.

### 3.6. Palladium ensemble and ligand effects

Alloy composition may significantly change its catalytic properties [76–80], and the three main effects to consider are: ensemble, ligand, and strain effects [80,81]. The ensemble effect involves changes in the chemical composition at the adsorption site, while the ligand effect results from electronic modifications due to variations in chemical composition in the vicinity of the active site. The strain effect, on the other hand, arises from differences in interatomic distances between different metals with distinct lattice constants. Especially, for single atom adsorbates, the ensemble exerts the most substantial impact on adsorbate binding to an alloy surface, while the strain effect remains minimal.

**Table 6**
Selectivity descriptors of ethylene calculated at T = 230 K and partial pressure of 1 bar pressure for all the reaction components, on a $Pd_1Ag$ SAA surface.

| Descriptor | Free energy (eV) |
|---|---|
| Acetylene | |
| $\Delta G_{TS}$ | 0.37 |
| $\Delta G_{des}$ | 0.51 |
| $\Delta\Delta G^{AC}$ | −0.14 |
| Ethylene | |
| $\Delta G_{TS}$ | 0.35 |
| $\Delta G_{des}$ | 0.21 |
| $\Delta\Delta G^{ET}$ | 0.14 |
| Selective for ET | Yes |

**Table 7**
Adsorption energies for the different organic molecules on the Pd dimer and Pd sublayer SAA surfaces as well as activation energies of the first hydrogenation step for AC and PA and their derivatives. All values are in eV.

| Surface | $E_{ads}$ | $E_{act}$ |
|---|---|---|
| Pd dimer | | |
| AC | −1.44 | 0.45 |
| ET | −0.92 | 0.59 |
| PA | −1.71 | 0.52 |
| ST | −1.49 | 0.55 |
| DPA | −1.86 | – |
| CST | −1.76 | – |
| TST | −1.83 | – |
| Pd sublayer | | |
| AC | −0.75 | 0.30 |
| ET | −0.86 | 0.44 |
| PA | −1.32 | 0.44 |
| ST | −1.42 | 0.33 |
| DPA | −1.61 | – |
| CST | −1.85 | – |
| TST | −1.96 | – |

Instead of generating various surfaces with different concentrations of Pd, we are investigating the ensemble and ligand effects separately using two PdAg model surfaces: one featuring a Pd dimer, representing the ensemble effect, and another with a Pd sublayer, representing the ligand effect. We will exclude the strain effect from our analysis. The Pd dimer is designed to minimize ensemble effect within the SAA system. The ligand effect is typically less pronounced than the ensemble effect [80,81], so we will amplify it by converting the entire first sublayer from Ag into Pd. This conversion ensures an uniform ligand effect across the top surface layer. Both of these model systems have a similar impact on the d-band centre [82,83] of the surface Pd atom. Specifically, the d-band centre of the dilute $Pd_1Ag$ SAA is −0.85 eV, and this value increases to −0.79 eV for both the Pd dimer and the Pd sublayer configurations.

Fig. 5 presents adsorption structures and Table 7 the adsorption energies of the different organic molecules on Pd dimer and Pd sublayer surfaces. Additionally, Fig. 6 provides a visual comparison of adsorption energies on pure Ag and all the PdAg SAA surfaces. It is evident that higher Pd content typically leads to more exothermic adsorption energies. However, as the adsorbate size increases, the ability of the SAA to bind them more strongly diminishes. The reduction is most pronounced in the case of the Pd dimer and least significant in the Pd sublayer surface. Moving from $Pd_1Ag$ SAA and the Pd sublayer surfaces to the Pd dimer, the preferred adsorption site changes from an on-top position at the Pd-atom to a bridge site situated between the two Pd-atoms. On the $Pd_1Ag$ SAA and on the Pd sublayer surfaces, the double-bonded molecules bind more strongly than the triple-bonded

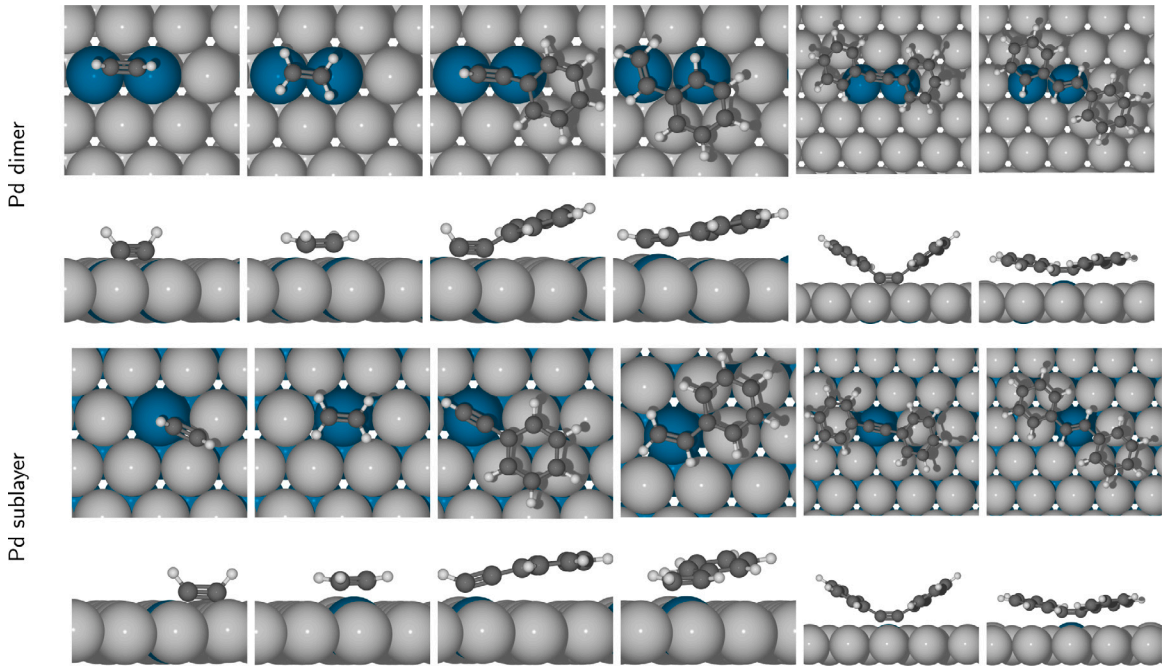


**Fig. 5.** From left to right, top and side views of the optimal adsorption geometries of AC, ET, PA, ST, DPA and TST Pd dimer (upper row) and Pd sublayer (lower row) PdAg SAA surfaces.

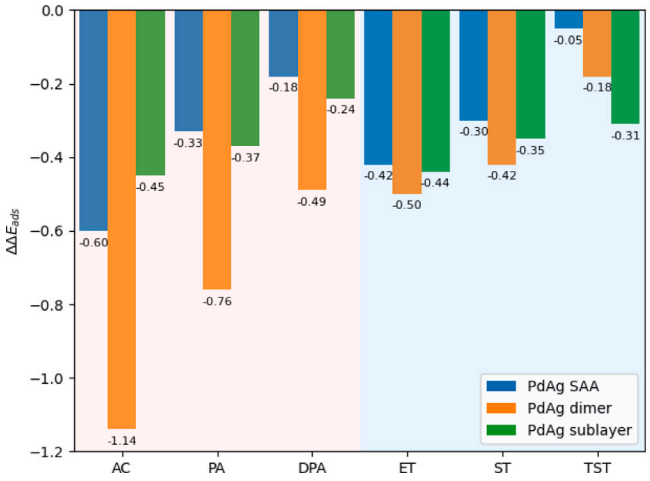


**Fig. 6.** The difference in adsorption energies between Ag(111) and PdAg, $E_{ads}^{PdAg} - E_{ads}^{Ag}$, at different Pd-content. The red and blue backgrounds depict an alkyne and alkene species, respectively. The more exothermic the adsorption energy is on PdAg compared to Ag, the more negative the difference $E_{ads}^{PdAg} - E_{ads}^{Ag}$.

one. Conversely, on the Pd dimer, the reverse trend is observed. This shift is noteworthy, as favouring alkynes over alkenes enables the Pd dimer to selectively hydrogenate the alkynes.

As discussed earlier, the selectivity in the hydrogenation of AC on the $Pd_1Ag$ SAA is due to the more favourable adsorption energy of AC over ET. However, this selectivity does not hold for PA and DPA, where the double-bonded products (ST and CST/TST) bind more strongly to the surface. The adsorption behaviour on the SAA surface aligns with the trend observed for the Ag(111) surface, where molecules with a double bond bind more strongly than molecules with a triple bond. The opposite is observed on Pd(111). Therefore, it is plausible that a Pd-ensemble would lead to selective adsorption on PdAg, favouring the triple-bonded variety.

The activation energies for the initial hydrogenation steps of various molecules are also detailed in Table 7. For ET, both the Pd dimer and the Pd sublayer configurations exhibit a higher hydrogenation barrier compared to AC, whereas the barriers for PA are higher than for ST on Pd sublayer. Overall, the hydrogenation barriers are lower on the Pd sublayer and higher on the Pd dimer compared to the $Pd_1Ag$ SAA. Interestingly, the selectivity descriptors for PA (see Table 8) indicate that the Pd dimer surface demonstrates a preference towards partial hydrogenation (i.e. $\Delta\Delta G^{PA} < \Delta\Delta G^{ST}$), while the Pd sublayer lack this selectivity ($\Delta\Delta G^{PA} > \Delta\Delta G^{ST}$). This behaviour mainly arises from the fact that adsorption on the Pd dimer provides additional stabilization for the triple-bonded species relative to the double-bonded ones. For a more comprehensive analysis of the influence of Pd composition on selectivity at various pressures and temperatures, please refer to Tables S3 to S10 in the Supplementary Information.

## 4. Conclusion

In this study, we explored the hydrogenation pathways for PA on PdAg SAA, and for comparison, also on monometallic Pd and Ag surfaces. Additionally, we investigated how the molecule size and the ensemble and ligand effects influence the hydrogenation thermodynamics and kinetics on the alloy surfaces.

The PA hydrogenation process is found to be inactive on neat Ag. Despite relatively low hydrogenation barriers, the adsorption of the reactants on Ag(111) is too weak to occur at process temperatures. In contrast, while the Pd surface exhibits slightly higher hydrogenation barriers, the adsorption of the reactants on Pd(111) is notably exothermic. Due to the strong adsorption, the surface coverage of the reactants is high. Consequently, the high surface coverage significantly weakens the binding of ST, while PA adsorption energy remains largely unaffected. This difference in adsorption energies likely contributes to Pd's selectivity towards partial hydrogenation of PA into ST.

According to our calculations, the $Pd_1Ag$ SAA surpasses the activity of the neat Ag host. The SAA promotes $H_2$ dissociation and enhances the binding of all considered reactant molecules. However, while the $Pd_1Ag$ SAA exhibits selectivity towards AC hydrogenation to ET, it does

**Table 8**
Selectivity descriptors at T = 350 K for acetylene/phenylacetylene and ethylene/styrene hydrogenation at partial pressures of 1 bar for all the reactants, on the Pd dimer and Pd sublayer surfaces. All values are given in eV.

| | Pd dimer | Pd sublayer | $Pd_1Ag$ SAA |
|---|---|---|---|
| Acetylene | | | |
| $\Delta G_{TS}$ | 0.41 | 0.31 | 0.36 |
| $\Delta G_{des}$ | 0.77 | 0.02 | 0.23 |
| $\Delta\Delta G^{AC}$ | −0.35 | 0.30 | 0.13 |
| Ethylene | | | |
| $\Delta G_{TS}$ | 0.52 | 0.42 | 0.35 |
| $\Delta G_{des}$ | 0.19 | −0.15 | −0.09 |
| $\Delta\Delta G^{ET}$ | 0.33 | 0.57 | 0.44 |
| Selective for ET | Yes | No | No |
| Phenylacetylene | | | |
| $\Delta G_{TS}$ | 0.48 | 0.37 | 0.37 |
| $\Delta G_{des}$ | 0.83 | 0.05 | 0.14 |
| $\Delta\Delta G^{PA}$ | −0.35 | 0.32 | 0.24 |
| Styrene | | | |
| $\Delta G_{TS}$ | 0.48 | 0.26 | 0.32 |
| $\Delta G_{des}$ | 0.45 | 0.03 | 0.14 |
| $\Delta\Delta G^{ST}$ | 0.03 | 0.23 | 0.18 |
| Selective for ST | Yes | No | No |

not demonstrate selectivity for PA hydrogenation to ST according to the theoretical considerations. The kinetic behaviour of these two processes is similar with the key difference being how AC and PA adsorb the surface. Furthermore, ST binds more strongly compared to PA, while AC is able to adopt a more stable adsorption geometry than ET. This disparity in relative stability facilitates the selective hydrogenation of AC, even on the $Pd_1Ag$ SAA surface.

We also investigated the influence of higher Pd concentration using a Pd dimer and Pd sublayer models for the PdAg SAA system, representing ensemble and ligand effects, respectively. Both models enhance the adsorption of studied molecules, but the Pd dimer displays stronger binding to alkyne species compared to alkene species, while on the Pd sublayer alkenes bind more strongly. On the Pd dimer, alkynes can adsorb to a bridge site between the Pd dimer atoms and this change in the adsorption mode of PA facilitates selective hydrogenation.

The calculations examining the influence of the size of the reactant molecule on binding show that the PdAg SAA generally improves reactant binding but this effect diminishes for larger molecules. This is an important observation, since many computational studies on SAAs focus on small molecules or single atoms binding to isolated active sites. Therefore, extending these results to larger molecules is not straightforward. Our study underscore the significance of reactant molecule size and surface ensemble effects in the realm of single-atom alloy catalysis, especially considering the chemical nature of large organic molecules binding with potentially multipoint adsorption to the surface of SAA catalysts.

## CRediT authorship contribution statement

**Hanan H. Ibrahim:** Writing – original draft, Visualization, Investigation, Formal analysis. **Timo Weckman:** Writing – review & editing, Validation, Supervision, Data curation, Conceptualization. **Dmitry Yu. Murzin:** Writing – review & editing, Conceptualization. **Karoliina Honkala:** Writing – review & editing, Supervision, Project administration, Funding acquisition, Conceptualization.

## Data availability

Supplementary Information is available. Supplementary Information related to this article can be found online at https://doi.org/10.1016/j.jcat.2024.115523. All the optimized structures and reaction pathways are available for free at IDA Fairdata service, https://doi.org/10.23729/4fb60b0f-fe7b-4337-b5b0-af3a13f11b6d.

## Acknowledgements

The electronic structure calculations were made possible by computational resources provided by the CSC – IT Center for Science, Espoo, Finland (https://www.csc.fi/en/). HI and KH acknowledges Business Finland project Synjet and Finnish Research council, Finland project number 21000047181 for funding this work. TW and KH acknowledges Jane and Aatos Erkko Foundation, Finland for the funding for the LACOR project.

## References

[1] L. Xiang, H. Feng, M. Liu, X. Zhang, G. Fan, F. Li, Surface defect-induced site-specific dispersion of Pd nanoclusters on $TiO_2$ nanoparticles for semihydrogenation of phenyl acetylene, ACS Appl. Nano Mater. 4 (2021) 4688–4698.
[2] Y. Liu, W. Guo, X. Li, P. Jiang, N. Zhang, M. Liang, Copper single-atom-covered Pt nanoparticles for selective hydrogenation of phenylacetylene, ACS Appl. Nano Mater. 4 (2021) 5292–5300.
[3] G. Iucci, V. Carravetta, G. Paolucci, A. Goldoni, M. Russo, G. Polzonetti, Phenylacetylene adsorption on Rh(100): a photoemission and photoabsorption investigation, Chem. Phys. 310 (2005) 43–49.
[4] S.-S. Chen, U. by Staff, Styrene, in: Kirk-Othmer Encyclopedia of Chemical Technology, John Wiley & Sons, Ltd, 2006.
[5] P.V. Markov, I.S. Mashkovsky, G.O. Bragina, J. Wärnå, E.Y. Gerasimov, V.I. Bukhtiyarov, A.Y. Stakheev, D.Y. Murzin, Particle size effect in liquid-phase hydrogenation of phenylacetylene over Pd catalysts: Experimental data and theoretical analysis, J. Chem. Eng. 358 (2019) 520–530.
[6] S. Dominguezdominguez, A. Berenguermurcia, D. Cazorlaamoros, A. Linares-solano, Semihydrogenation of phenylacetylene catalyzed by metallic nanoparticles containing noble metals, J. Catal. 243 (2006) 74–81.
[7] P. Weerachawanasak, O. Mekasuwandumrong, M. Arai, S.-I. Fujita, P. Praserthdam, J. Panpranot, Effect of strong metal–support interaction on the catalytic performance of $Pd/TiO_2$ in the liquid-phase semihydrogenation of phenylacetylene, J. Catal. 262 (2009) 199–205.
[8] J. Hu, Z. Zhou, R. Zhang, L. Li, Z. Cheng, Selective hydrogenation of phenylacetylene over a nano-$Pd/\alpha$-$Al_2O_3$ catalyst, J. Mol. Catal. A Chem. 381 (2014) 61–69.
[9] A.V. Rassolov, G.O. Bragina, G.N. Baeva, N.S. Smirnova, A.V. Kazakov, I.S. Mashkovsky, A.Y. Stakheev, Liquid-phase hydrogenation of internal and terminal alkynes on Pd–Ag/$Al_2O_3$ catalyst, Kinet. Catal. 60 (2019) 642–649.
[10] G. Kyriakou, M.B. Boucher, A.D. Jewell, E.A. Lewis, T.J. Lawton, A.E. Baber, H.L. Tierney, M. Flytzani-Stephanopoulos, E.C.H. Sykes, Isolated metal atom geometries as a strategy for selective heterogeneous hydrogenations, Science 335 (2012) 1209–1212.
[11] T. Zhang, A.G. Walsh, J. Yu, P. Zhang, Single-atom alloy catalysts: Structural analysis, electronic properties and catalytic activities, Chem. Soc. Rev. 50 (2021) 569–588.
[12] L. Jiang, K. Liu, S.-F. Hung, L. Zhou, R. Qin, Q. Zhang, P. Liu, L. Gu, H.M. Chen, G. Fu, N. Zheng, Facet engineering accelerates spillover hydrogenation on highly diluted metal nanocatalysts, Nat. Nanotechnol. 15 (2020) 848–853.
[13] L. Zhang, M. Zhou, A. Wang, T. Zhang, Selective hydrogenation over supported metal catalysts: from nanoparticles to single atoms, Chem. Rev. 120 (2020) 683–733.
[14] R.T. Hannagan, G. Giannakakis, M. Flytzani-Stephanopoulos, E.C.H. Sykes, Single-atom alloy catalysis, Chem. Rev. 120 (2020) 12044–12088.
[15] W. Liu, H. Feng, Y. Yang, Y. Niu, L. Wang, P. Yin, S. Hong, B. Zhang, X. Zhang, M. Wei, Highly-efficient RuNi single-atom alloy catalysts toward chemoselective hydrogenation of nitroarenes, Nature Commun. 13 (2022) 3188.
[16] J. Liu, J. Shan, F. R. Lucci, S. Cao, E.C. H. Sykes, M. Flytzani-Stephanopoulos, Palladium–gold single atom alloy catalysts for liquid phase selective hydrogenation of 1-hexyne, Catal. Sci. Technol. 7 (2017) 4276–4284.
[17] M. Ouyang, K.G. Papanikolaou, A. Boubnov, A.S. Hoffman, G. Giannakakis, S.R. Bare, M. Stamatakis, M. Flytzani-Stephanopoulos, E.C.H. Sykes, Directing reaction pathways via in situ control of active site geometries in PdAu single-atom alloy catalysts, Nature Commun. 12 (2021) 1549.
[18] R. Svensson, H. Grönbeck, Site communication in direct formation of $H_2O_2$ over Single-Atom Pd@Au Nanoparticles, J. Am. Chem. Soc. 145 (2023) 11579–11588.
[19] G. Giannakakis, M. Flytzani-Stephanopoulos, E.C.H. Sykes, Single-atom alloys as a reductionist approach to the rational design of heterogeneous catalysts, Acc. Chem. Res. 52 (2019) 237–247.
[20] A.V. Rassolov, I.S. Mashkovsky, G.O. Bragina, G.N. Baeva, P.V. Markov, N.S. Smirnova, J. Wärnå, A.Y. Stakheev, D.Y. Murzin, Kinetics of liquid-phase diphenylacetylene hydrogenation on “single-atom alloy” Pd-Ag catalyst: Experimental study and kinetic analysis, Mol. Catal. 506 (2021) 111550.

[21] M.B. Boucher, M.D. Marcinkowski, M.L. Liriano, C.J. Murphy, E.A. Lewis, A.D. Jewell, M.F.G. Mattera, G. Kyriakou, M. Flytzani-Stephanopoulos, E.C.H. Sykes, Molecular-scale perspective of water-catalyzed methanol dehydrogenation to formaldehyde, ACS Nano 7 (2013) 6181–6187.

[22] P. Aich, H. Wei, B. Basan, A.J. Kropf, N.M. Schweitzer, C.L. Marshall, J.T. Miller, R. Meyer, Single-Atom Alloy Pd–Ag catalyst for selective hydrogenation of acrolein, J. Phys. Chem. C 119 (2015) 18140–18148.

[23] G.X. Pei, X.Y. Liu, A. Wang, A.F. Lee, M.A. Isaacs, L. Li, X. Pan, X. Yang, X. Wang, Z. Tai, K. Wilson, T. Zhang, Ag alloyed Pd single-atom catalysts for efficient selective hydrogenation of acetylene to ethylene in excess ethylene, ACS Catal. 5 (2015) 3717–3725.

[24] D.C. Upham, V. Agarwal, A. Khechfe, Z.R. Snodgrass, M.J. Gordon, H. Metiu, E.W. McFarland, Catalytic molten metals for the direct conversion of methane to hydrogen and separable carbon, Science 358 (2017) 917–921.

[25] X. Zhang, G. Cui, H. Feng, L. Chen, H. Wang, B. Wang, X. Zhang, L. Zheng, S. Hong, M. Wei, Platinum–copper single atom alloy catalysts with high performance towards glycerol hydrogenolysis, Nature Commun. 10 (2019) 5812.

[26] H.L. Tierney, A.E. Baber, J.R. Kitchin, E.C.H. Sykes, Hydrogen dissociation and spillover on individual isolated palladium atoms, Phys. Rev. Lett. 103 (2009) 246102.

[27] F.R. Lucci, M.T. Darby, M.F.G. Mattera, C.J. Ivimey, A.J. Therrien, A. Michaelides, M. Stamatakis, E.C.H. Sykes, Controlling hydrogen activation, spillover, and desorption with Pd–Au single-atom alloys, J. Phys. Chem. Lett. 7 (2016) 480–485.

[28] M.T. Darby, M. Stamatakis, A. Michaelides, E.C.H. Sykes, Lonely atoms with special gifts: Breaking linear scaling relationships in heterogeneous catalysis with single-atom alloys, J. Phys. Chem. Lett. 9 (2018) 5636–5646.

[29] M.T. Darby, R. Réocreux, E. Charles, H. Sykes, A. Michaelides, M. Stamatakis, Elucidating the stability and reactivity of surface intermediates on single-atom alloy catalysts, ACS Catal. 8 (2018) 5038–5050.

[30] H. Thirumalai, J.R. Kitchin, Investigating the reactivity of single atom alloys using density functional theory, Top. Catal. 61 (2018) 462–474.

[31] R.T. Hannagan, G. Giannakakis, R. Réocreux, J. Schumann, J. Finzel, Y. Wang, A. Michaelides, P. Deshlahra, P. Christopher, M. Flytzani-Stephanopoulos, M. Stamatakis, E.C.H. Sykes, First-principles design of a single-atom–alloy propane dehydrogenation catalyst, Science 372 (2021) 1444–1447.

[32] J. Schumann, Y. Bao, R.T. Hannagan, E.C.H. Sykes, M. Stamatakis, A. Michaelides, Periodic trends in adsorption energies around single-atom alloy active sites, J. Phys. Chem. Lett. 12 (2021) 10060–10067.

[33] G.-C. Zhao, Y.-Q. Qiu, C.-G. Liu, A systematic theoretical study of hydrogen activation, spillover and desorption in single-atom alloys, Appl. Catal. A: Gen 610 (2021) 117948.

[34] T.D. Spivey, A. Holewinski, Selective interactions between free-atom-like *d* -states in single-atom alloy catalysts and near-frontier molecular orbitals, J. Am. Chem. Soc. 143 (2021) 11897–11902.

[35] W. Li, S.E. Madan, R. Réocreux, M. Stamatakis, Elucidating the reactivity of oxygenates on single-atom alloy catalysts, ACS Catal. 13 (2023) 15851–15868.

[36] R.T. Hannagan, H.Y. Lam, R. Réocreux, Y. Wang, A. Dunbar, V. Lal, V. Çınar, Y. Chen, P. Deshlahra, M. Stamatakis, N.M. Eagan, E.C.H. Sykes, Investigating spillover energy as a descriptor for single-atom alloy catalyst design, J. Phys. Chem. Lett. 14 (2023) 10561–10569.

[37] I. Horiuti, M. Polanyi, Exchange reactions of hydrogen on metallic catalysts, J. Chem. Soc., Faraday trans. 30 (1934) 1164–1172.

[38] Y. Han, D. Peng, Z. Xu, H. Wan, S. Zheng, D. Zhu, $TiO_2$ supported Pd@Ag as highly selective catalysts for hydrogenation of acetylene in excess ethylene, Chem. Commun. 49 (2013) 8350.

[39] G.X. Pei, X.Y. Liu, X. Yang, L. Zhang, A. Wang, L. Li, H. Wang, X. Wang, T. Zhang, Performance of Cu-Alloyed Pd single-atom catalyst for semihydrogenation of acetylene under simulated front-end conditions, ACS Catal. 7 (2017) 1491–1500.

[40] M. Jørgensen, H. Grönbeck, Selective acetylene hydrogenation over single-atom alloy nanoparticles by kinetic Monte Carlo, J. Am. Chem. Soc. 141 (2019) 8541–8549.

[41] M.R. Ball, K.R. Rivera-Dones, E.B. Gilcher, S.F. Ausman, C.W. Hullfish, E.A. Lebrón, J.A. Dumesic, AgPd and CuPd catalysts for selective hydrogenation of acetylene, ACS Catal. 10 (2020) 8567–8581.

[42] W. Xie, J. Xu, Y. Ding, P. Hu, Quantitative studies of the key aspects in selective acetylene hydrogenation on Pd(111) by microkinetic modeling with coverage effects and molecular dynamics, ACS Catal. 11 (2021) 4094–4106.

[43] E. Vignola, S.N. Steinmann, A. Al Farra, B.D. Vandegehuchte, D. Curulla, P. Sautet, Evaluating the risk of C–C bond formation during selective hydrogenation of acetylene on palladium, ACS Catal. 8 (2018) 1662–1671.

[44] M.B. Boucher, B. Zugic, G. Cladaras, J. Kammert, M.D. Marcinkowski, T.J. Lawton, E.C.H. Sykes, M. Flytzani-Stephanopoulos, Single atom alloy surface analogs in $Pd_{0.18}Cu_{15}$ nanoparticles for selective hydrogenation reactions, Phys. Chem. Chem. Phys. 15 (2013) 12187–12196.

[45] Z. Wang, L. Yang, R. Zhang, L. Li, Z. Cheng, Z. Zhou, Selective hydrogenation of phenylacetylene over bimetallic Pd–Cu/$Al_2O_3$ and Pd–Zn/$Al_2O_3$ catalysts, Catal. Today 264 (2016) 37–43.

[46] L. Chen, B. Huang, X. Qiu, X. Wang, R. Luque, Y. Li, Seed-mediated growth of MOF-encapsulated Pd@Ag core–shell nanoparticles: Toward advanced room temperature nanocatalysts, Chem. Sci. 7 (2016) 228–233.

[47] A. Zharmagambetova, A. Auyezkhanova, E. Talgatov, A. Jumekeyeva, F. Buharbayeva, S. Akhmetova, Z. Myltykbayeva, J.M.L. Nieto, Synthesis of polymer protected Pd–Ag/ZnO catalysts for phenylacetylene hydrogenation, J. Nanopart. Res. 24 (2022) 236.

[48] J. Enkovaara, C. Rostgaard, J.J. Mortensen, J. Chen, M. Dułak, L. Ferrighi, J. Gavnholt, C. Glinsvad, V. Haikola, H.A. Hansen, H.H. Kristoffersen, M. Kuisma, A.H. Larsen, L. Lehtovaara, M. Ljungberg, O. Lopez-Acevedo, P.G. Moses, J. Ojanen, T. Olsen, V. Petzold, N.A. Romero, J. Stausholm-Møller, M. Strange, G.A. Tritsaris, M. Vanin, M. Walter, B. Hammer, H. Häkkinen, G.K.H. Madsen, R.M. Nieminen, J.K. Nørskov, M. Puska, T.T. Rantala, J. Schiøtz, K.S. Thygesen, K.W. Jacobsen, Electronic structure calculations with GPAW: A real-space implementation of the projector augmented-wave method, J. Phys.: Condens. Matter 22 (2010) 253202.

[49] A.H. Larsen, J.J. Mortensen, J. Blomqvist, I.E. Castelli, R. Christensen, M. Dułak, J. Friis, M.N. Groves, B. Hammer, C. Hargus, E.D. Hermes, P.C. Jennings, P.B. Jensen, J. Kermode, J.R. Kitchin, E.L. Kolsbjerg, J. Kubal, K. Kaasbjerg, S. Lysgaard, J.B. Maronsson, T. Maxson, T. Olsen, L. Pastewka, A. Peterson, C. Rostgaard, J. Schiøtz, O. Schütt, M. Strange, K.S. Thygesen, T. Vegge, L. Vilhelmsen, M. Walter, Z. Zeng, K.W. Jacobsen, The atomic simulation environment—a Python library for working with atoms, J. Phys.: Condens. Matter 29 (2017) 273002.

[50] J.P. Perdew, K. Burke, M. Ernzerhof, Generalized gradient approximation made simple, Phys. Rev. Lett. 77 (1996) 3865–3868.

[51] S. Grimme, J. Antony, S. Ehrlich, H. Krieg, A consistent and accurate *Ab Initio* parametrization of density functional dispersion correction (DFT-D) for the 94 elements H-Pu, J. Chem. Phys. 132 (2010) 154104.

[52] S. Grimme, S. Ehrlich, L. Goerigk, Effect of the damping function in dispersion corrected density functional theory, J. Comput. Chem. 32 (2011) 1456–1465.

[53] D.G.A. Smith, L.A. Burns, K. Patkowski, C.D. Sherrill, Revised damping parameters for the D3 dispersion correction to density functional theory, J. Phys. Chem. Lett. 7 (2016) 2197–2203.

[54] G. Henkelman, H. Jónsson, Improved tangent estimate in the nudged elastic band method for finding minimum energy paths and saddle points, J. Chem. Phys. 113 (2000) 9978–9985.

[55] G. Henkelman, B.P. Uberuaga, H. Jónsson, A climbing image nudged elastic band method for finding saddle points and minimum energy paths, J. Chem. Phys. 113 (2000) 9901–9904.

[56] E. Bitzek, P. Koskinen, F. Gähler, M. Moseler, P. Gumbsch, Structural relaxation made simple, Phys. Rev. Lett. 97 (2006) 170201.

[57] D.R. Lide, CRC Handbook of Chemistry and Physics, 89th ed., CRC Press, Boca Raton, FL, 2008.

[58] A.H. Larsen, J.J. Mortensen, J. Blomqvist, I.E. Castelli, R. Christensen, M. Dułak, J. Friis, M.N. Groves, B. Hammer, C. Hargus, et al., The atomic simulation environment—a Python library for working with atoms, J. Phys.: Condens. Matter 29 (27) (2017) 273002.

[59] C. Li, Z. Shao, M. Pang, C.T. Williams, X. Zhang, C. Liang, Carbon nanotubes supported mono- and bimetallic Pt and Ru catalysts for selective hydrogenation of phenylacetylene, Ind. Eng. Chem. Res. 51 (2012) 4934–4941.

[60] L. Xu, E.E. Stangland, M. Mavrikakis, Ethylene versus ethane: A DFT-based selectivity descriptor for efficient catalyst screening, J. Catal. 362 (2018) 18–24.

[61] L. Nykänen, K. Honkala, Density functional theory study on propane and propene adsorption on Pt(111) and PtSn alloy surfaces, J. Phys. Chem. C 115 (2011) 9578–9586.

[62] P. Ferrin, S. Kandoi, A.U. Nilekar, M. Mavrikakis, Hydrogen adsorption, absorption and diffusion on and in transition metal surfaces: A DFT study, Surf. Sci. 606 (7–8) (2012) 679–689.

[63] J. Greeley, M. Mavrikakis, Surface and subsurface hydrogen: adsorption properties on transition metals and near-surface alloys, J. Phys. Chem. B 109 (8) (2005) 3460–3471.

[64] H. Conrad, G. Ertl, E. Latta, Adsorption of hydrogen on palladium single crystal surfaces, Surf. Sci. 41 (2) (1974) 435–446.

[65] R. Réocreux, E.C.H. Sykes, A. Michaelides, M. Stamatakis, Stick or spill? scaling relationships for the binding energies of adsorbates on single-atom alloy catalysts, J. Phys. Chem. Lett. 13 (2022) 7314–7319.

[66] C. Morin, D. Simon, P. Sautet, Chemisorption of benzene on Pt(111), Pd(111), and Rh(111) metal surfaces: a structural and vibrational comparison from first principles, J. Phys. Chem. B 108 (2004) 5653–5665.

[67] R.S. Shamsiev, F.O. Danilov, DFT modeling of mechanism of hydrogenation of phenylacetylene into styrene on a Pd(111) surface, Kinet. Catal. 59 (2018) 333–338.

[68] S. Tuokko, P.M. Pihko, K. Honkala, First principles calculations for hydrogenation of acrolein on Pd and Pt: chemoselectivity depends on steric effects on the surface, Angew. Chem., Int. Ed. 128 (2016) 1702–1706.

[69] P. Tiruppathi, J.J. Low, A.S. Chan, S.R. Bare, J.M. Randall, Density functional theory study of the effect of subsurface H, C, and Ag on $C_2H_2$ hydrogenation on Pd(111), Catalysis Today 165 (2011) 106–111.

[70] B. Yang, R. Burch, C. Hardacre, G. Headdock, P. Hu, Influence of surface structures, subsurface carbon and hydrogen, and surface alloying on the activity and selectivity of acetylene hydrogenation on Pd surfaces: A density functional theory study, J. Catal. 305 (2013) 264–276.
[71] H.-H. Wei, C.H. Yen, H.-W. Lin, C.-S. Tan, Synthesis of bimetallic Pd–Ag colloids in $CO_2$-expanded hexane and their application in partial hydrogenation of phenylacetylene, J. Supercrit. Fluids 81 (2013) 1–6.
[72] M. Muir, M. Trenary, Adsorption of CO to characterize the structure of a Pd/Ag(111) single-atom alloy surface, J. Phys. Chem. C 124 (2020) 14722–14729.
[73] M.A. Van Spronsen, K. Daunmu, C.R. O'Connor, T. Egle, H. Kersell, J. Oliver-Meseguer, M.B. Salmeron, R.J. Madix, P. Sautet, C.M. Friend, Dynamics of surface alloys: rearrangement of Pd/Ag(111) induced by CO and $O_2$, J. Phys. Chem. C 123 (2019) 8312–8323.
[74] A.V. Rassolov, G.O. Bragina, G.N. Baeva, I.S. Mashkovsky, A.Y. Stakheev, Alumina-supported palladium–silver bimetallic catalysts with single-atom $Pd_1$ sites in the liquid-phase hydrogenation of substituted alkynes, Kinet. Catal. 61 (2020) 869–878.
[75] A.V. Rassolov, G.O. Bragina, G.N. Baeva, N.S. Smirnova, A.V. Kazakov, I.S. Mashkovsky, A.V. Bukhtiyarov, Y.V. Zubavichus, A.Y. Stakheev, Formation of isolated single-atom $Pd_1$ sites on the Surface of Pd–Ag/$Al_2O_3$ bimetallic catalysts, Kinet. Catal. 61 (2020) 758–767.
[76] S. García, L. Zhang, G.W. Piburn, G. Henkelman, S.M. Humphrey, Microwave synthesis of classically immiscible rhodium–silver and rhodium–gold alloy nanoparticles: highly active hydrogenation catalysts, ACS Nano 8 (2014) 11512–11521.
[77] N. Takehiro, P. Liu, A. Bergbreiter, J.K. Nørskov, R.J. Behm, Hydrogen adsorption on bimetallic PdAu(111) surface alloys: Minimum adsorption ensemble, ligand and ensemble effects, and ensemble confinement, Phys. Chem. Chem. Phys. 16 (2014) 23930–23943.
[78] H. Li, G. Henkelman, Dehydrogenation selectivity of ethanol on close-packed transition metal surfaces: a computational study of monometallic, Pd/Au, and Rh/Au Catalysts, J. Phys. Chem. C 121 (2017) 27504–27510.
[79] H. Li, L. Luo, P. Kunal, C.S. Bonifacio, Z. Duan, J.C. Yang, S.M. Humphrey, R.M. Crooks, G. Henkelman, Oxygen reduction reaction on classically immiscible bimetallics: a case study of RhAu, J. Phys. Chem. C 122 (2018) 2712–2716.
[80] H. Li, K. Shin, G. Henkelman, Effects of ensembles, ligand, and strain on adsorbate binding to alloy surfaces, J. Chem. Phys. 149 (2018) 174705.
[81] P. Liu, J.K. Nørskov, Ligand and ensemble effects in adsorption on alloy surfaces, Phys. Chem. Chem. Phys. 3 (2001) 3814–3818.
[82] B. Hammer, J.K. Nørskov, Why gold is the noblest of all the metals, Nature 376 (1995) 238–240.
[83] S. Jiao, X. Fu, H. Huang, Descriptors for the evaluation of electrocatalytic reactions: d-band theory and beyond, Adv. Funct. Mater. 32 (2022) 2107651.